Nanotechnology

PAPER

Surface plasmon assisted laser ablation of stainless steel

To cite this article: Liu Lu *et al* 2019 *Nanotechnology* **30** 305401

View the article online for updates and enhancements.

IOP ebooks™

Bringing you innovative digital publishing with leading voices to create your essential collection of books in STEM research.

Start exploring the collection - download the first chapter of every title for free.

This content was downloaded from IP address 129.237.90.142 on 05/07/2019 at 17:03

IOP Publishing Nanotechnology
Nanotechnology 30 (2019) 305401 (7pp) https://doi.org/10.1088/1361-6528/ab1806

Surface plasmon assisted laser ablation of stainless steel

Liu Lu[1,2], Ruifa Tan[1], Daifen Chen[3], Yanqun Tong[1], Xiaohong Yan[1], Maogang Gong[2,4] and Judy Z Wu[2,4]

[1] School of Mechanical Engineering, Jiangsu University, Zhenjiang 212013, People's Republic of China
[2] Department of physics and Astronomy, The University of Kansas, Lawrence 66044, United States of America
[3] School of Energy and Power, Jiangsu University of Science and Technology, Zhenjiang 212013, People's Republic of China

E-mail: gmg@ujs.edu.cn and jwu@ku.edu

Received 10 January 2019, revised 5 March 2019
Accepted for publication 10 April 2019
Published 3 May 2019

Abstract

Colloidal Au nanoparticles (NPs) were decorated on stainless steel for surface plasmon enhanced laser ablation. A comparative study of the laser ablation efficiency was carried out on stainless steel samples with and without the Au NPs decoration at a variable pulsed laser fluence and laser pulse number. Higher ablation efficiency was clearly demonstrated in the former as illustrated from the larger diameter, maximum depth and the cross-sectional area of the crater generated by the laser ablation under the same conditions. Additionally, both the maximum depth and efficiency enhancement were found to depend on the laser fluence and pulse number. The maximum enhanced ablation efficiency of 36% based on the cross-sectional area of the crater was obtained at 1 pulse number of laser fluence 1.53 J cm^{-2}. The efficiency enhancement of laser ablation is attributed to the highly enhanced surface plasmon field at the interface between Au NPs and stainless steel.

Keywords: laser ablation, surface plasmon, efficiency enhancement, near field, stainless steel

(Some figures may appear in colour only in the online journal)

1. Introduction

The light-induced coherent electron resonance that occurs at the surface of metals, known as surface plasmon, can provide extraordinary capabilities in light management through confinement and enhancement of electromagnetic field of the incident light near the metal surface [1–3]. Since electron plasmonic oscillations constitute an electrical current on metal surface that heats up the material by means of the Ohmic loss, a key consequence is the resonant plasmonic absorption of incident photons to produce local heating of the plasmonic structure. This can enable a series of applications taking advantages of such plasmonic Ohmic heating [4, 5]. For example, the plasmonic loss induced heating was recently adopted to address a long-standing challenge in the field of plasmon enhanced optical trapping to rapidly load the plasmonic trap on-demand in long range [6]. The loss induced plasmonic heating could also play a role in optical data storage and encryption [7], plasmonic photo-thermal therapy [8, 9], the conversion of solar energy to electricity [10], the enhanced photoelectrochemical water splitting [11, 12] and infrared thermal photodetector [13].

Among others, an important application of the plasmonic loss induced heating is near-field laser processing technology [14]. For instances, plasmonic Au nanoparticles (NPs) can be used in visible laser ablation for fabrication of two dimensional nanohole arrays with the hole diameter of 30 nm, significantly exceeding the optical diffraction limit [15]. this near-field ablation process has also been illustrated to be successful for imaging the near-field light distribution with a resolution below 20 nm [16]. Another published work about melting the material precisely in the regions of plasmonic hotspots also proves the effect of surface plasmon on laser ablation [17]. Moreover, a near-field laser ablation system

[4] Authors to whom any correspondence should be addressed.

 © 2019 IOP Publishing Ltd Printed in the UK

was developed for the analysis of inorganic solid samples with a nanometer resolution [18]. With the assistance of plasmonic resonant of Au bowtie nano antennas, an ablation mechanism called gentle ablation (electrostatic ablation) since its ablation rate is several orders of magnitude lower than that of thermal ablation, was observed on SiO_2 [19–21].

Besides the mentioned applications due to the localized surface plasmons, the propagation surface plasmons also play an important role in laser ablation. For example, the surface plasmon polariton dominantly contributes to the formation of the nanograting on GaN films by the ablation of femtosecond laser pulses [22]. Similarly, the influence of propagation surface plasmons on the formation of subwavelength periodic ripples on Au films was also reported recently [23]. In addition to the metal nanostructures, the transparent dielectric particle can act as micro-lens for near-field laser ablation [24, 25]. However, the mechanisms for near-field laser ablation by dielectric particle and metal plasmonic nanostructures are different. Here, the absorbed incident energy can enter the particle and finally focus on the interaction of the transparent particle on the substrate, the energy flow can be explained based on the dipole approximation and classical Mie theory [26, 27].

To improve the laser processing performance, continuous efforts have been focused on both precision and efficiency. Laser processing mediated by plasmonic near-field has proved to be a promising method to realize high-precision processing. Most of the previous works on near-field laser ablation are conducted on glass or silica substrates with a primary focus on the precision of the ablation pattern. In this paper, we present the investigation of the laser ablation of the 304 stainless steels without and with plasmonic Au NPs decoration using visible laser pulses under different conditions of laser fluence and pulse number. Importantly, we show the localized surface plasmon can enhance efficiency of the laser ablation illustrated in increased diameter, depth and profile area of the ablated craters. Considering the plasmonic resonance frequency can be tuned by selecting the Au NP diameter [28], the optimal absorption of the Au NPs was controlled to be at 532 nm through controlling the Au NP diameter to about 45 nm, consistent to the wavelength of the laser for an optimal efficiency.

2. Experimental details

2.1. Preparation and deposition of Au NPs on the 304 stainless steel

A seed solution of 2.6 nm diameter Au colloids was prepared by adding 0.1 ml of 1% aqueous sodium citrate solution into 10 ml of 0.01% aqueous $HAuCl_4{\cdot}3H_2O$ solution with vigorous stirring for 1 min 0.1 ml of fresh 0.075% $NaBH_4$ in 1% sodium citrate was added afterwards and the colloidal solution was stirred for an additional 5 min. For preparation of Au NPs with diameter about 45 nm, 200 ml of 0.01% $HAuCl_4{\cdot}3H_2O$ was brought to boiling under microwave heating [29]. To this solution was added 2 ml of freshly prepared seed colloids and 0.8 ml of 1% aqueous sodium citrate. Boiling was continued for an additional 6 min in microwave oven. After polishing and cleaning 304 steel slides (25 × 20 × 1.5 mm), a half of the steel was immersed in a dilute solution of 3-aminopropyltrimethoxysilane (APTMS) (5 g APTMS in 40 g CH3OH) for 12 h and rinsed with copious amounts of CH_3OH upon removal. Then, half part of the prepared APTMS-coated steel slide was subsequently immersed in Au colloidal solution for 12 h to assemble the Au NPs on the surface of the stainless steel, followed by rinsing with deionized water. Before the coating of Au NPs, the stainless less was chemically and mechanically polished, achieving a roughness level on its surface of 10 nm.

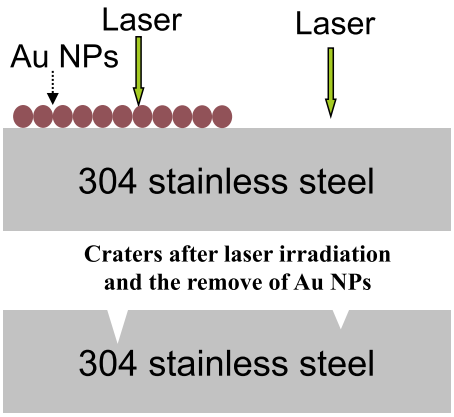

Figure 1. Schematic of the experiment.

2.2. Laser irradiation and measurements

Figure 1 depicts the experiment schematic. Pulsed laser of the wavelength 532 nm was irradiated on both bare (right) and Au NPs covered (left) stainless steel. The model of used pulsed laser is RLA1504-AG/A. The diameter of the laser beam is around 100 μm and the pulse duration is 2.5 ns, the frequency of follow-up pulses is 1 KHz. Here, the laser fluence of a single pulse was changed in 1.02, 1.27 and 1.53 J cm^{-2}. The pulse number was altered in the range of 1, 2, 5 and 10.

Absorption spectra of Au NPs in solution were measured using an HP 8453 diode array spectrophotometer. The morphologies as well as the depth profiles of the craters formed by the laser irradiation on the stainless steel samples were measured using confocal scanning laser microscopy. Before the crater morphology measurement, the samples were subjected to ultrasonic cleaning in ethanol to remove the Au NPs as shown in figure 1 (bottom).

2.3. Simulation

The simulation of the electric field distribution for Au NPs coated stainless steel was carried out using a commercial finite-difference time domain package (Lumerical Solutions, Inc.). The simulated model is consisted of single Au NP on stainless steel slide. The diameter of the Au NP was 45 nm and a laser irradiation was selected at 532 nm wavelength. A mesh size of 0.1 nm was chosen in the simulation. The dielectric functions of the Au NP and stainless steel were taken from Palik (1998) [30].

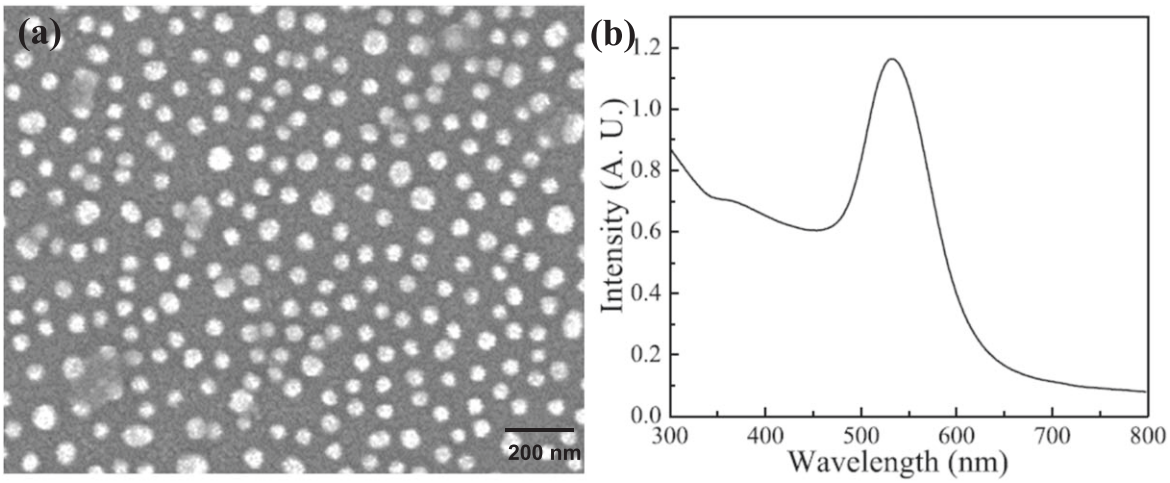

Figure 2. (a) SEM image of the self-assembled Au NPs array on the Fe slide. (b) Absorption spectra of the Au colloids solution.

3. Discussion and results

The most widely used synthetic technique for Au NPs is reduction of boiling $HAuCl_4$ aqueous solution directly by sodium citrate, which is called Frens method [31]. This approach is effective for the preparation of spherical Au NPs with diameter less than 30 nm. In this work, Au NPs with larger diameter of 45 nm were obtained in a microwave oven using a citrate seeding growth procedure, which is similar to that developed by the group of Natan [32]. Figure 2(a) illustrates a representative FESEM image of the Au NPs assembled on the stainless steel slide. Overall, the Au NPs are better dispersed on the sample surface. The Au NPs are mostly spherical, their diameter d is about 45 nm, as shown in FESEM image. It is known that the excitation of the surface plasmon of Au NPs would account for the enhancement of the electromagnetic field around the surface of the metal NPs. The resonant frequency of the surface plasmon can be characterized in the absorption spectrum shown in figure 2(b). The absorption peak at 532 nm is the frequency of the localized surface plasmon resonance of Au NPs. This absorption peak is controlled equal to the excitation laser of 532 nm wavelength, with the goal to most efficiently utilize the surface plasmon local field around the Au NPs for the following laser ablation experiment.

Figures 3(a)–(d) and (e)–(h) show respectively the scanning laser images of the craters formed on the stainless steel without and with Au NPs coating. Here, the laser fluence was set at 1.53 J cm^{-2}, while the pulse number was altered in 1, 2, 5 and 10. Besides, the depths profiles of the craters are also present on the bottom of the scanning laser images. From figure 3, one can observe that all the craters are halo-shape bumps with an outer rim. The observed crater morphology can be attributed the surface melting under the laser beam during the laser ablation process, which results in the excitation of convective fluxes within the liquid layer. Thermo-capillary and chemi-capillary forces are two main origins that lead to the changes in the surface tension [33]. Since the incident optical field has a Gaussian-like distribution, the temperature decreases from the center of the molten zone to its edge. For a uniform distributed material concentration, the temperature gradient causes an outward flow of the molten materials to the edge, causing the formation of the outer rim. When the laser fluence is high enough, a strong evaporation takes place in the central region that generates recoil pressure on the molten materials, leading to a halo structure in the crater center. Therefore, we can also observe the sputtered and molten materials around the crater. As the images in figure 3 show, the morphologies of the craters formed without and with Au NPs look similar under the same laser ablation conditions.

However, the dimensions of the craters differ considerably for the two cases. As illustrated from the depth profiles shown in figure 3, the diameters of the craters can be estimated from the distance between the two solid (figures 3(a)–(d), bare stainless steel) or dashed (figures 3(e)–(h), with assistance of the Au NPs) yellow vertical lines. The diameters of the craters on the former are respectively about 33.6, 32.0, 32.0 and 33.6 μm for the pulse number of 1, 2, 5 and 10. The observed comparable crater diameters suggest the effect of the pulse number on the diameter of the crater is negligible. With assistance of the Au NPs during the laser irradiation, the craters' diameters increase to 37.1, 35.0, 37.0 and 37.9 μm for the pulse number 1, 2, 5 and 10, as shown in the figures 3(e)–(h). This indicates that the plasmonic Au NPs in laser ablation would cause the diameter of the crater enlarged by 3–5 μm, which is a 9%–16% increase. Besides the change of the diameter, the crater's depth was also found to increase due to the introduction of the Au NPs. To clearly describe this behavior, figure 4 shows the maximum crater depth as a function of the pulses number under different laser fluence. At the laser fluence of 1.02 J cm^{-2} (figure 4(a)), the maximum crater depth on bare steel is 1.02 μm for a single laser pulse, and it increases to 1.27 μm on Au NPs coated steel. This corresponds to a 25% enhancement. Such an enhancement with the assistance of the Au NPs can also be observed at other laser ablation conditions with different laser fluence and pulse number. To quantify the influence of Au NPs, the normalized enhancement factor γ for the crater's depth can be calculated from: $\gamma = (h_{Au} - h_{bare})/h_{bare}$ and the result for different conditions is included in figure 4(d). At a given laser fluence, the γ decreases monotonically with the pulse number.

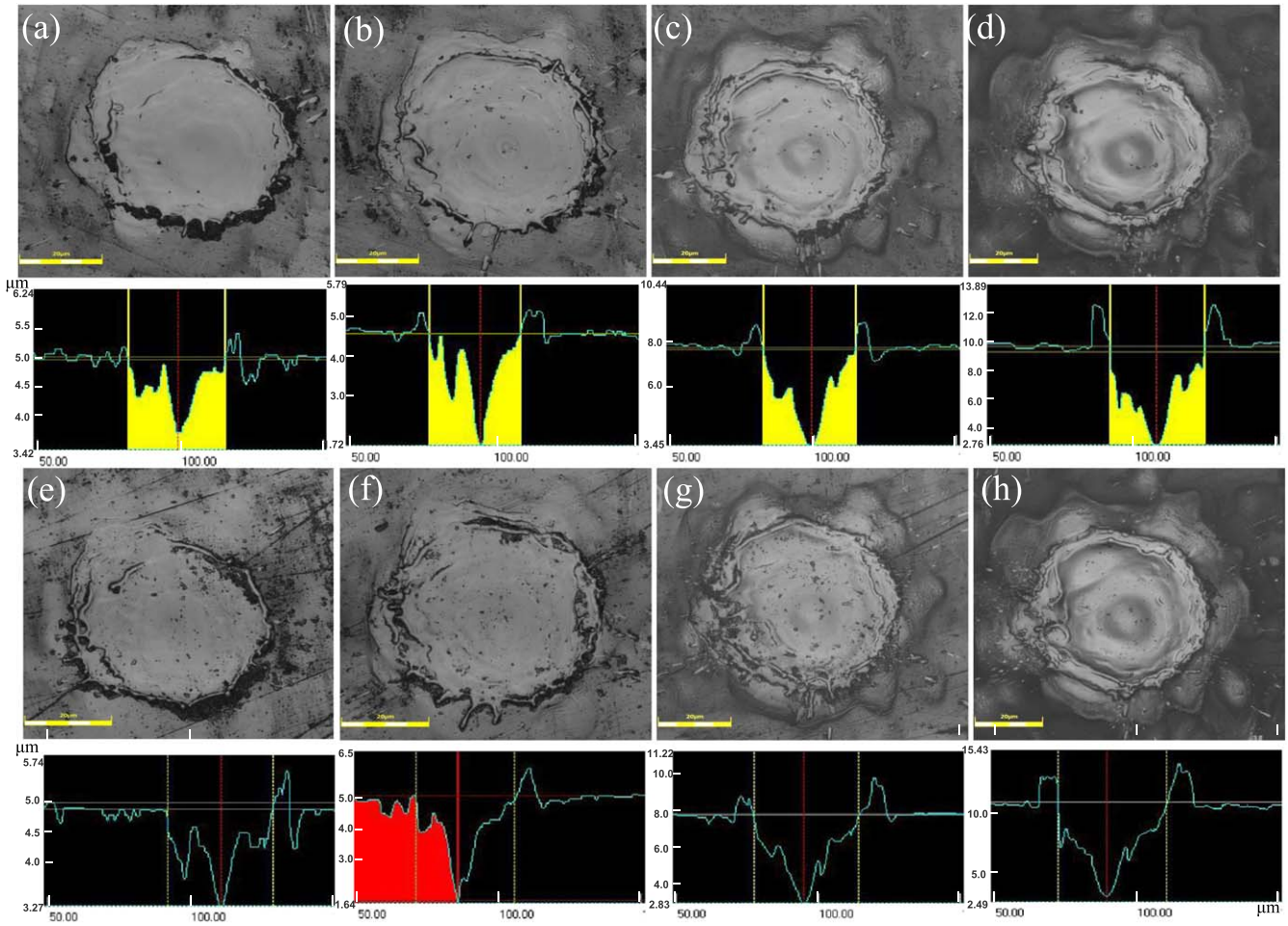

Figure 3. Laser scanning images of the craters after laser ablation at laser fluence 1.53 J cm^{-2} with different pulse numbers: (a), (e) 1; (b), (f) 2; (c), (g) 5; and (d), (h) 10. The images (a)–(d) correspond to the sample of the bare steel slide, while images (e)–(h) are the other half steel slides with Au NPs participation in laser irradiation. The corresponding height profiles were shown on the bottom of the laser scanning images.

For example, at the laser fluence of 1.02 J cm^{-2} (black line), γ decreases from 24.5% at a single pulse to 4.3% at 10 pulses. This behavior may be explained by the morphology variation and probable removal of Au NPs by the first laser pulse. Figure 4(d) also demonstrates that the descent rate of the enhancement with the increasing pulse number shows a sharpest decrease when laser fluence is 1.02 J cm^{-2}, this rate slows down with the laser fluence increases. Besides, with the change of laser fluence from 1.02 to 1.53 J cm^{-2} at a single pulse number, the enhancement factor is largest at the least laser fluence of 1.02 J cm^{-2} and decreases with the increasing laser fluence.

To quantitatively compare the amount of ablated material under the conditions with and without Au NPs, we define ablation factor β, which is the cross-sectional area of the profile of the crater shown in figure 3. Figures 5(a)–(c) depict the ablation factor β dependence on the laser fluence and pulse number. As the figure 5 demonstrated, the ablation factor is larger when the plasmonic Au NPs were decorated on the stainless steel. Considering the craters are almost central symmetric, it is reasonable to conclude that the amount of ablated material is increased by the participation of Au NPs in the laser ablation. In another word, the plasmonic Au NPs, and possibly other plasmonic nanostructures decorated in the stainless steel surface, can enhance the efficiency of the laser ablation of the steel. The efficiency enhancement ψ is defined as the $\psi = (\beta_{\mathrm{Au}} - \beta_{\mathrm{bare}})/\beta_{\mathrm{bare}}$, and the results of ψ as a function of laser pulse number under different laser fluence is shown in figure 5(d). The factor ψ is found to decrease with the increasing pulse number, and it increases with the increasing laser fluence. When laser fluence is 1.53 J cm^{-2}, the factors ψ are all above 26% in the pulse number ranging from 1–10, reaching the maximum value of 36% at 1 pulse number.

To reach the goal of employing plasmonic nanostructure as a controlled tool for industrial laser ablation, it is essential to understand the relation between the plasmonic nanostructure and the ablation process itself. In the bare steel case, laser ablation of steel is defined as the removal of material from a solid target (steel) by direct absorption of the photon energy by steel. The intensity of absorbed energy may depend on the material and its surface morphology. However, for the stainless steel with Au NPs assembled, the Au NPs would greatly absorb the excitation light, when irradiated by the

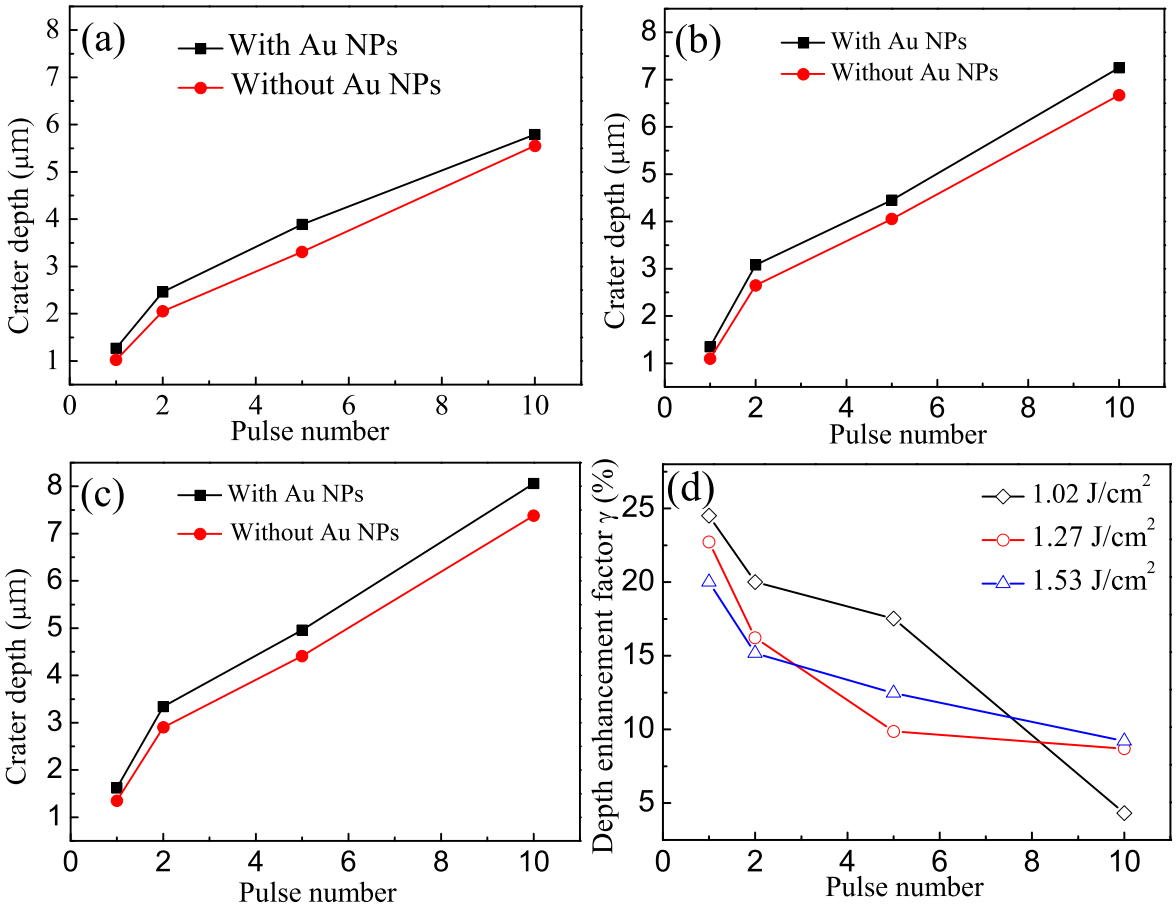

Figure 4. Maximum depth of the craters versus different laser fluence (a) 1.02 J cm^{-2}, (b) 1.27 J cm^{-2} and (c) 1.53 J cm^{-2} and pulse number. The curves in (d) are the normalized depth enhancement factor γ dependent on the laser fluence and pulse number.

laser with the wavelength near the surface plasmon frequency of the Au NPs, producing a highly enhanced scattering electromagnetic field. To contrast the absorption efficiency of the steel with and without Au NPs, figure 6 shows the reflectivity of the steel with and without Au NPs. From figure 6, it can be observed that the reflectivity of bare steel is almost linearly increasing with the wavelength. However, when coated by Au NPs, the reflectivity of the steel greatly decreases over the measured range, showing a pit ranging from 510–600 nm. This phenomenon is supposed to be contributed by the surface plasmon resonance of the Au NPs [34]. Note that the resonance peak for Au NPs is red-shifted due to the change of dielectric environment, when compared to that shown in figure 2(b). Figure 7 shows the $(E/E_0)^2$ of the local electric field of Au NP with diameter 45 nm on steel. It can be seen that there is a dramatic field enhancement, which can substantially surpass the incident field strength as much as to 1000 folds on the edge the Au NP. Because the Au NPs possess free carriers, the surface plasmon local field would unavoidably result in heating the particle itself and the surrounding medium [35]. The former can be described by electron dynamics, coherent acoustic lattice vibrations, melting and evaporation from the particle surface. The latter is described by photo-medium interaction, resulting in heating of the surroundings. This will allow the photon energy to be more uniformly focused on the surface of the steel so a larger portion of the absorbed photon energy can be used for ablation. This explains the observed higher ablation efficiency in this work through the comparison of the amount of the ablated material in Au NP coated steel as compared to the uncoated one. This will also cause that the larger the incident laser fluence is, the more the enhancement field is. Consequently, as indicated by the result in figure 6(d), the efficiency enhancement is large for laser fluence at 1.53 J cm^{-2}.

4. Conclusions

The localized surface plasmon enhanced efficiency of the laser ablation was investigated on 304 stainless steel with and without Au NPs coating using a pulsed laser of 2.5 ns pulse duration and 532 nm wavelength. The participation of Au NPs during the laser ablation was found to cause the diameter of the ablation craters enlarged by 9%–16%, the maximum depth of the crater enhanced above 20% at single pulse number. This leads to the cross-sectional area of the crater increased in all present conditions on samples with Au NPs. The enhancement was found to depend on the laser fluence and pulse number. Based on the cross-sectional area, the maximum efficiency of 36% was obtained at a single laser pulse of laser fluence 1.53 J cm^{-2}. This result indicates surface plasmonic resonance induced by Au NPs is beneficial to laser ablation efficiency by

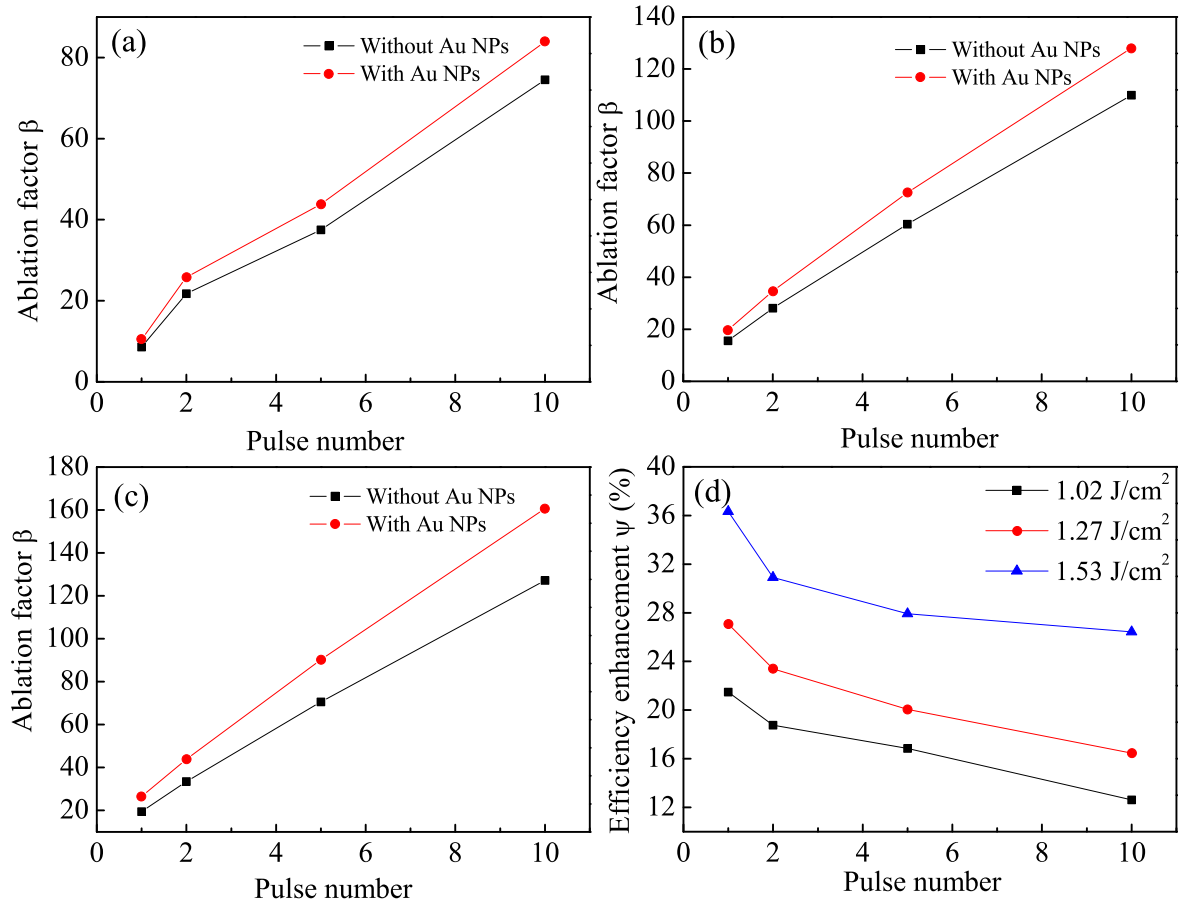

Figure 5. Cross-sectional area of the craters versus different laser fluence (a) 1.02 J cm^{-2}, (b) 1.27 J cm^{-2} and (c) 1.53 J cm^{-2} and pulse number. The curves in (d) are efficiency enhancement factor ψ dependent on the laser fluence and pulse number.

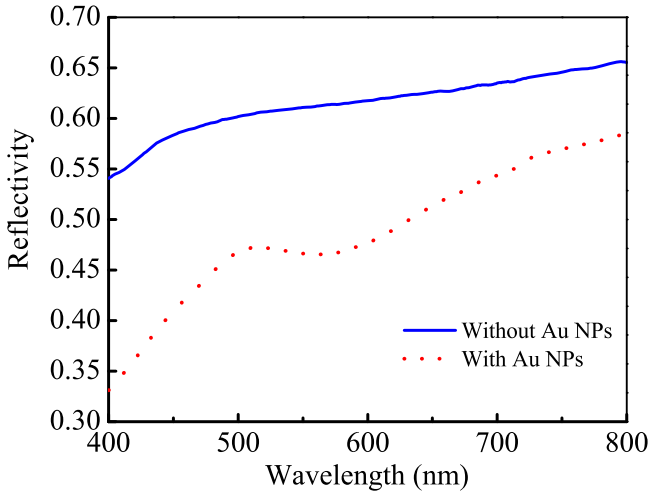

Figure 6. Reflectivity spectrum of the stainless steel with and without the coating of Au NPs.

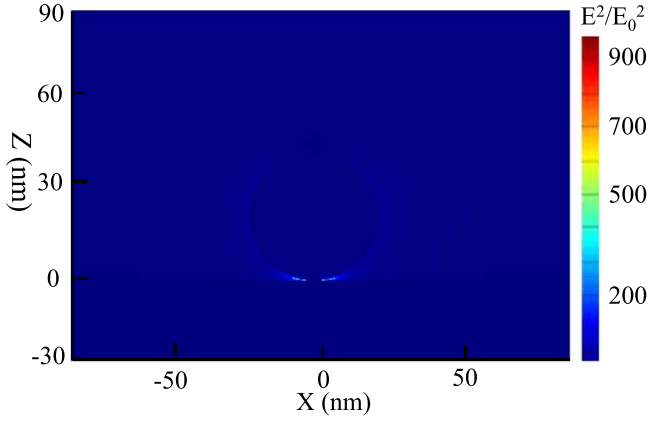

Figure 7. The simulated surface plasmon filed distribution of single Au NP on steel slide. The intensity of the field is described in $(E/E_0)^2$.

confining the incident laser electromagnetic field (far field) to an evanescent field of enhanced amplitude by a factor 1000 localized on the surface layer of the stainless steel. This localized field can provide additional energy in heating the Au NP itself and the surrounding medium, when compared to the case of the bare stainless steel reference samples.

Acknowledgments

This work is funded by National Natural Science Foundation of China (No. 91750112, 11204107 and No. 51775253). JW acknowledges supports from ARO contract No. W911NF-16-1-0029 and NSF contract No. NSF-DMR-1508494.

ORCID iDs

Maogang Gong https://orcid.org/0000-0002-2031-781X

References

[1] Liu Z X, Jiang M L, Hu Y L, Lin F, Shen B, Zhu X and Fang Z H 2018 Scanning cathodoluminescence microscopy: applications in semiconductor and metallic nanostructures *Opto-Electron. Adv.* **1** 180007–11

[2] Xu D, Xiong X, Wu L, Ren X F, Ching E P, Guo G C, Gong Q H and Xiao Y F 2018 Quantum plasmonics: new opportunity in fundamental and applied photonics *Adv. Opt. Photonics* **10** 703–56

[3] Chen Y *et al* 2018 Quantum plasmonic N00N state in a silver nanowire and its use for quantum sensing *Optica* **5** 1229–35

[4] Ndukaife J C, Shalaev V M and Boltasseva A 2016 Plasmonics-turning loss into gain. The optical losses associated with plasmonic materials could be used in applications *Science* **351** 334–5

[5] Baffou G and Quidant R 2014 Nanoplasmonics for chemistry *Chem. Soc. Rev.* **43** 3898–907

[6] Ndukaife J C, Kildishev A V, Nnanna A G A, Shalaev V M, Wereley S T and Boltasseva A 2016 Long-range and rapid transport of individual nano-objects by a hybrid electrothermoplasmonic nanotweezer *Nat. Nanotechnol.* **11** 53–60

[7] Roxworthy B J, Bhuiya A M, Inavalli V V, Chen H and Toussaint K C Jr 2014 Multifunctional plasmonic film for recording near-field optical intensity *Nano Lett.* **14** 4687–93

[8] Mackey M A, Ali M R K, Austin L A, Near R D and El-Sayed M A 2014 The most effective gold nanorod size for plasmonic photothermal therapy: theory and *in vitro* experiments *J. Phys. Chem.* B **118** 1319–26

[9] He Y L *et al* 2018 Exocytosis of gold nanoparticle and photosensitizer from cancer cells and their effects on photodynamic and photothermal processes *Nanotechnology* **29** 116603–38

[10] Xu G W, Lu R T, Liu J W, Chiu H Y, Hui R Q and Wu J Z 2014 Photodetection based on ionic liquid gated plasmonic ag nanoparticle/graphene nanohybrid field effect transistors *Adv. Opt. Mater.* **2** 729–36

[11] Sun K, Madsen K, Andersen P, Bao W, Sun Z and Wang D 2012 Metal on metal oxide nanowire Co-catalyzed Si photocathode for solar water splitting *Nanotechnology* **23** 194013–22

[12] Wei Y F, Ke L, Kong J H, Liu H, Jiao Z H, Lu X H, Du H J and Sun X W 2012 Enhanced photoelectrochemical water-splitting effect with a bent ZnO nanorod photoanode decorated with Ag nanoparticles *Nanotechnology* **23** 235401–8

[13] Tong J C, Suo F, Ma J H Z, Tobing L Y M, Qian L and Zhang D H 2019 Surface plasmon enhanced infrared photodetection *Opto-Electron. Adv.* **2** 180026

[14] Terakawa M and Nedyalkov N N 2016 Near-field optics for nanoprocessing *Adv. Opt. Technol.* **5** 17–28

[15] Yamada K, Narita C, Kumaresan R, Shinohara T, Terakawa M and Tsuboi Y 2017 Nanofabrication of high throughput 30 nm hole 2D arrays by a simple visible laser ablation technique *Appl. Surf. Sci.* **420** 868–72

[16] Kolloch A, Leiderer P, Ibrahimkutty S, Issenmann D and Plech A 2012 Structural study of near-field ablation close to plasmon-resonant nanotriangles *J. Laser Appl.* **24** 042105–7

[17] Valev V K *et al* 2012 Plasmon-Enhanced sub-wavelength laser ablation: plasmonic nanojets *Adv. Mater.* **24** Op29–35

[18] Jabbour C, Lacour J L, Tabarant M, Semerok A and Chartier F 2016 Development of a tip enhanced near-field laser ablation system for the sub-micrometric analysis of solid samples *J. Anal. At. Spectrom.* **31** 1534–41

[19] Shi L P *et al* 2017 Self-optimization of plasmonic nanoantennas in strong femtosecond fields *Optica* **4** 1038–43

[20] Plech A, Kotaidis V, Lorenc M and Boneberg J 2006 Femtosecond laser near-field ablation from gold nanoparticles *Nat. Phys.* **2** 44–7

[21] Kolloch A, Geldhauser T, Ueno K, Misawa H, Boneberg J, Plech A and Leiderer P 2011 Femtosecond and picosecond near-field ablation of gold nanotriangles: nanostructuring and nanomelting *Appl. Phys.* A **104** 793–9

[22] Miyaji G and Miyazaki K 2016 Fabrication of 50 nm period gratings on GaN in air through plasmonic near-field ablation induced by ultraviolet femtosecond laser pulses *Opt. Express* **24** 4648–53

[23] Zhou K, Jia X, Jia T Q, Cheng K, Cao K Q, Zhang S A, Feng D H and Sun Z R 2017 The influences of surface plasmons and thermal effects on femtosecond laser-induced subwavelength periodic ripples on Au film by pump-probe imaging *J. Appl. Phys.* **121** 104301–7

[24] Afanasiev A, Bredikhin V, Pikulin A, Ilyakov I, Shishkin B, Akhmedzhanov R and Bityurin N 2015 Two-color beam improvement of the colloidal particle lens array assisted surface nanostructuring *Appl. Phys. Lett.* **106** 183102–4

[25] Brodoceanu D, Alhmoud H Z, Elnathan R, Delalat B, Voelcker N H and Kraus T 2016 Fabrication of silicon nanowire arrays by near-field laser ablation and metal-assisted chemical etching *Nanotechnology* **27** 075301–8

[26] Wang Z B, Luk B S, Hong M H, Lin Y and Chong T C 2004 Energy flow around a small particle investigated by classical Mie theory *Phys. Rev.* B **70** 035418

[27] Huang S M, Hong M H, Luk B S, Zheng Y W, Dong W D, Lu Y F and Chong T C 2002 Pulsed laser-assisted surface structuring with optical near-field enhanced effects *J. Appl. Phys.* **92** 2459

[28] Lu L, Chen D F, Sun F W, Ren X F, Han Z F and Guo G C 2010 Photoluminescence quenching and enhancement of CdSe/PMMA composite on Au colloids *Chem. Phys. Lett.* **492** 71–6

[29] Lu L, Chen D F, Zhao G M, Ren X F and Guo G C 2010 Temperature and excitation wavelength dependent of surface-Plasmon-mediated emission from CdSe Nanocrystals *J. Phys. Chem.* C **114** 18435

[30] Palik E D 1998 *Handbook of Optical Constants of Solids* (New York: Academic) 1, 286–9

[31] Frens G 1972 Particle-size and sol stability in metal colloids *Kolloid Z. Z. Polym.* **250** 736

[32] Brown K R, Walter D G and Natan M J 2000 Seeding of colloidal Au nanoparticle solutions: II. Improved control of particle size and shape *Chem. Mater.* **12** 306–13

[33] Hong M H, Wang Z B, Lukyanchuk B S, Tan L S and Chong T C 2006 From transparent particle light enhancement to laser nanoimprinting *J. Laser Micro Nanoeng.* **1** 61–6

[34] Jia K, Khaywah M Y, Li Y G, Bijeon J L, Adam P M, Deturche R, Guelorget B, Francois M, Louarn G and Ionescu R E 2014 Strong improvements of localized surface plasmon resonance sensitivity by using Au/Ag bimetallic nanostructures modified with polydopamine films *ACS Appl. Mater. Interfaces* **6** 219–27

[35] Hashimoto S, Werner D and Uwada T 2012 Studies on the interaction of pulsed lasers with plasmonic gold nanoparticles toward light manipulation, heat management, and nanofabrication *J. Photochem. Photobiol.* C **13** 28–54